TECHNICAL PAPER

Bearing failure and influence factors analysis of metal-to-composite bolted joints at high temperature

Salam Abdus[1] · Xiaoquan Cheng[1] · Wenjun Huang[3] · Altaf Ahmed[2] · Renwei Hu[1]

Abstract

In this paper, experiments were conducted to study the tensile performance of metal-to-composite bolted joints at room temperature and 250 °C. Furthermore, numerical models were developed to simulate tensile behavior of the joint. After achieving a decent validation between numerical models and experimental results, more detailed studies were conducted through finite element models to find out the influence of temperature, bolt material, the thickness of composite laminate and stacking sequence on tensile properties of the joint at room temperature and 250 °C. The research showed that temperature significantly affects the bearing strength of the joint. Around 42–50% decrease in bearing strength was observed at 250 °C as compared to room temperature. Stacking sequence variations have a little more effect on bearing strength at higher temperature than at room temperature. With the change of stacking sequences, around 11–24% variation in bearing strength was observed at 250 °C as compared to 8–20% at room temperature.

Keywords Metal-to-composite bolted joint · FEM · Tensile performance · Elevated temperature

1 Introduction

There is a remarkable rise in the use of composite material in almost every industry, especially military and commercial aircraft, satellites and space launchers [1–3]. When equated with other materials, composite materials have higher specific strength and rigidity, chemical and corrosion resistance and higher resistance for temperature [4–7].

Due to the limitation of design, manufacturing, usage and maintenance, the connection or joint structures are unavoidable. As the efficiency of composite structures is primarily influenced by the efficiency of the joint, research to precisely predict the tensile properties of the composite joint is very crucial [8–12]. Bolted joints can transfer high loads and are

Technical Editor: Paulo de Tarso Rocha de Mendonça, Ph.D.

✉ Xiaoquan Cheng
  xiaoquan_cheng@buaa.edu.cn

1 School of Aeronautical Science and Engineering, Beihang University, Beijing 100191, China

2 School of Management Sciences and Engineering, Beihang University, Beijing 100191, China

3 AVIC China Helicopter Research and Development Institute, Jingdezhen 333001, China

less sensitive to environmental conditions when compared with bonded joints, which exhibit higher sensitivity to environmental conditions and high interlaminar stresses [13]. Many factors affect the bearing strength of composite joints like ply sequence, clamping torque, environment temperature, geometry parameters, etc. [14–18].

Ibrahim Fadil Soykok et al. [19] investigated a decrease of 70% in the failure load of the double-bolted single-lap glass fiber/epoxy joint at 80 °C. They also observed that there is no temperature effect on the failure mode of joint, i.e., same failure was observed at room and high temperatures due to the reason that failure modes are mainly affected by material and geometric parameters. Turvey and Sana [20] experimentally studied the effects of geometry and temperature (40–80 °C) on characteristic failure stress to facilitate the preliminary design for double-lap single-bolted tension joint. They made tables that can help the designer to check the change in stresses with the change of edge-to-diameter ratio at a particular temperature. Zu et al. [16] studied the temperature effects (from 40 to 120 °C) on the bearing response of fiber metal laminate joints. Their results showed a decrease of up to 40% at 120 °C as compared to room temperature.

As many researchers investigated the tensile properties of the bolted composite-to-metal joints at room temperature

only, the research content at high temperature, especially above 200 °C, is minimal. At elevated temperature, thermal expansion mismatch between composite and metal, residual thermal stresses, change in properties of material and change in fit conditions of joint greatly influence the tensile properties of the joint. To take full advantages of the composite bolted joints and to optimize the design, it is necessary to carry out experimental and theoretical research of the bolted connections at elevated temperatures. Main failure modes in bolted composite joints are bearing, cleavage, net tension and shear-out failures. Bearing failure normally happens because of compressive stresses generated by the compressive load near the region of bolt and composite hole that bring the composite plate to nonlinear behavior [12, 21, 22].

In this study, specimens were manufactured for experimental testing, and 3D finite element models were established for numerical analysis. Once the numerical model closely agreed with experimental results, the detailed study was conducted to investigate the effect of different factors on the strength of CCF300/GW300 bolted joint at room temperature and higher temperatures.

2 Experimental procedure

According to ASTM D5961M standard, 14 specimens of CCF300/GW300 carbon fiber-reinforced composite-to-aluminum bolted joints were manufactured. Based on ply sequences and geometry, samples were divided into two groups. The laminate thickness of group 1 was 4.5 mm and bolt-hole diameter was 6 mm. The laminate thickness of group 2 laminate was 2.4 mm and bolt-hole diameter was 5 mm. The ply sequence of group 1 laminates was $[0_2/\pm 45/90/0/\pm 45/0_3/\pm 45/90/0]_S$ and ply sequence of group 2 laminates was $[0_2/\pm 45/0_2/90/0]_S$. Four specimens from each group were tested experimentally at room conditions and remaining tested at 250 °C. The details of group 1 specimens are in Fig. 1. The details of group 2 specimens were almost the same as that of group 1, but the bolt-hole diameter was 5 mm and the laminate thickness was 2.4 mm. The material of the metallic plate was aluminum, while the

bolt material was chosen to be titanium. 3.5 N-m bolt torque was applied on all the specimens. Laminates' mechanical and thermal properties [23] are given in Tables 1 and 2, respectively. The bolt and metal plate material properties are given in Table 3 [23].

Instron 8802 (250 kN) was used to perform all the experiments. The machine loading rate was chosen to be 1 mm/min for all tests. The details of test setups at the room and high temperature are shown in Fig. 2. The temperature rising was carried out in a self-heating chamber with the capability of 350 °C maximum temperature increase. The apparatus was set to increase at a rate of 30 °C/min. Once the temperature of specimen reached the required level, the machine was kept at this temperature for 5 min before the loading was started.

3 Numerical model

3.1 Damage simulation

A progressive damage model (PDM) of metal-to-composite bolted joint was established. The calculation process of PDM mainly includes stress–strain calculation, the initial damage criterion and material property degradation. For composite material, the suitable damage criteria are used to precisely refer to the state of the material and predict whether

Table 1 Composite laminates mechanical properties at room temperature

Elastic		Strength	
Group	Value	Group	Value (MPa)
E_1 (GPa)	126	X_T	1260
E_2 (GPa)	9.76	X_C	1370
E_3 (GPa)	9.76	Y_T	24.7
G_{12}, G_{13} (GPa)	5.21	Y_C	178
G_{23} (GPa)	3.36	S_{12}	57.4
v_{12}, v_{13}	0.3	S_{23}	103
v_{23}	0.36	S_{13}	57.4

Fig. 1 Geometry details of group 1 specimens **a** front view and **b** top view
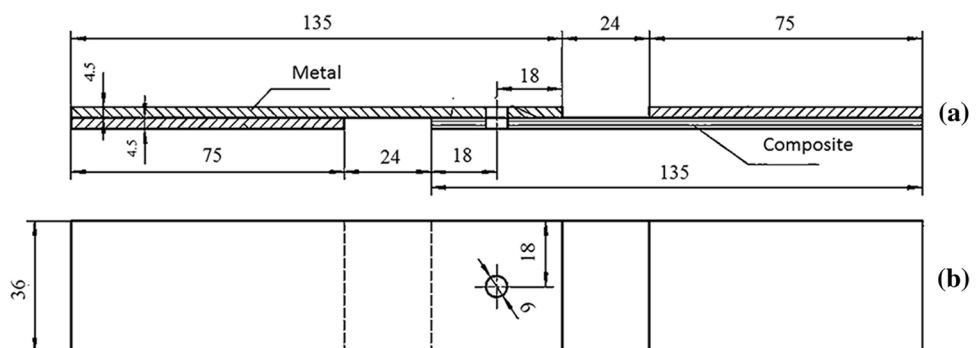
Table 2 Thermal properties of laminates

Group	Value at RT	Value at 250 °C
Longitudinal heat transfer coefficient [k_{11} (W/m °C)]	9.6	9.8
Heat transfer coefficient in transverse and through thickness direction [k_{22}, k_{33} (W/m °C)]	1.1	1.2
Density (kg/m^3)	1600	1600
Longitudinal thermal expansion coefficient [α_{11} ($\times 10^{-6}$/°C)]	0.03	0.05
Thermal expansion coefficient in transverse and through thickness direction [α_{22}, α_{33} ($\times 10^{-6}$/°C)]	23.5	26
Specific heat [C (kJ/(kg °C))]	1.2	1.2

Table 3 Material properties of bolt and metal plate

Property name	Bolt	Metal plate
Modulus of elasticity [E (GPa)]	110	70.6
Poisson's ratio (v)	0.29	0.3
Yield strength [Y_s (MPa)]	825	356
Thermal expansion coefficient [α ($\times 10^{-6}$/°C)]	8.6	21.6
Heat transfer coefficient [k (W/m °C)]	6.7	130
Specific heat [C (kJ/(kg °C))]	0.526	0.960

it will fail. Then, the values of material elastic constants were reduced according to the different types of damage. The strength calculation terminated as soon as the bearing capacity of the laminate is rapidly decreased, at this time,

the structure completely fails. The damage analysis of the laminate takes into account fiber tension and compression failures, matrix compression, and tension failure, matrix/fiber shear failure and delamination in compression and tension. The PDM calculation process is shown in Fig. 3.

3.1.1 Laminate damage

Many scholars have researched to establish a series of different types of strength criteria for anisotropic composite materials theoretically, experimentally and through FE simulation [24–26]. In this study, Hashin failure rules [27] are used to forecast laminate damage. The classification criteria for damage based on various forms of damage are as follows:

Fig. 2 Heating and testing setup **a** heating chamber and **b** at room temperature testing machine

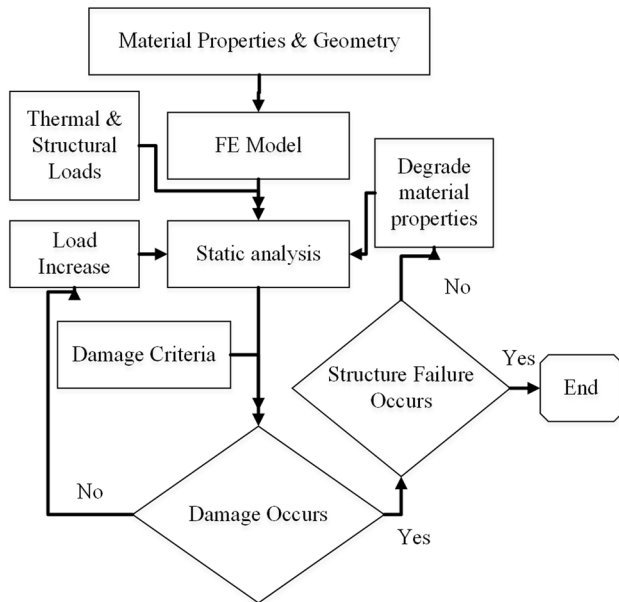(a)   (b)

Fig. 3 PDM damage calculation process in Abaqus

(a) Fiber tensile damage

$$\left(\frac{\sigma_1}{X_T}\right)^2 + \left(\frac{\tau_{12}}{S_{12}}\right)^2 + \left(\frac{\tau_{13}}{S_{13}}\right)^2 \geq 1 \qquad (1)$$

(b) Fiber compressive damage

$$\left(\frac{\sigma_1}{X_C}\right)^2 \geq 1 \qquad (2)$$

(c) Matrix tensile cracking

$$\left(\frac{\sigma_2}{Y_T}\right)^2 + \left(\frac{\tau_{12}}{S_{12}}\right)^2 + \left(\frac{\tau_{23}}{S_{23}}\right)^2 \geq 1 \qquad (3)$$

(d) Matrix compressive cracking

$$\left(\frac{\sigma_2}{Y_C}\right)^2 + \left(\frac{\tau_{12}}{S_{12}}\right)^2 + \left(\frac{\tau_{23}}{S_{23}}\right)^2 \geq 1 \qquad (4)$$

(e) Fiber–matrix shear failure

$$\left(\frac{\sigma_1}{X_C}\right)^2 + \left(\frac{\tau_{12}}{S_{12}}\right)^2 + \left(\frac{\tau_{13}}{S_{13}}\right)^2 \geq 1 \qquad (5)$$

(f) Delamination in tension

$$\left(\frac{\sigma_3}{Y_T}\right)^2 + \left(\frac{\tau_{12}}{S_{12}}\right)^2 + \left(\frac{\tau_{13}}{S_{13}}\right)^2 \geq 1 \qquad (6)$$

Table 4 Stiffness degradation criteria

Damage form	Degradation criteria
Fiber breakage	All material properties $\times 0.07$
Matrix cracking	$E_{22} = 0.2E_{22}$, $G_{13} = 0.2G_{13}$, $G_{23} = 0.2G_{23}$, $v_{13} = 0.2v_{13}$, $v_{23} = 0.2v_{23}$
Fiber/matrix shear failure	$G_{12} = 0.2G_{12}$, $v_{12} = 0.2v_{12}$
Delamination	$E_{33} = 0.2E_{33}$, $G_{13} = 0.2G_{13}$, $G_{23} = 0.2G_{23}$, $v_{13} = 0.2v_{13}$, $v_{23} = 0.2v_{23}$

(g) Delamination in compression

$$\left(\frac{\sigma_3}{Y_C}\right)^2 + \left(\frac{\tau_{12}}{S_{12}}\right)^2 + \left(\frac{\tau_{13}}{S_{13}}\right)^2 \geq 1 \qquad (7)$$

In the formula, σ_1, σ_2 and σ_3 are normal stresses in positive coordinate system 1, 2 and 3, respectively. τ_{12}, τ_{13} and τ_{23} are shearing stresses. X_T and X_C represent strengths in the tensile and compressive direction of fiber, respectively. Y_T and Y_C represent tensile and compressive strengths in transverse direction. Z_T and Z_C indicate tensile/compressive strength of the matrix, and S_{12}, S_{13} and S_{23} are in-plane and interlaminar shear strengths.

3.1.2 Degradation of composite laminates

In the experiment, the composite material will still bear some loading after damage. To simulate this behavior in FEM, many researchers develop degradation guidelines for the reduction of material stiffness. The selection of criteria for failure has a major impact on the accuracy of material degradation models. In this study, reduction factors proposed by Camanho, Papanikos and Tan [28–30] are used. Table 4 shows the degradation rules.

3.2 Model details

Owing to the geometric and loading symmetry, half of the model was constructed for thermal and structural analysis. Elements selected for thermal load calculations were DC3D8. Figure 4 shows the FE model and applied boundary conditions for the thermal model, where "T" is the temperature applied and "h" is the heat convection coefficient.

Figure 5 shows the boundary conditions and the 3D FE model for structural analysis. By using C3D8R three-dimensional solid elements, the FE model was developed with three parts as a metal plate, composite laminates and bolt. C3D8R elements are eight-node brick elements having reduced integration (1 integration point). Each node of

Fig. 4 Thermal finite element model details **a** top view and **b** front view
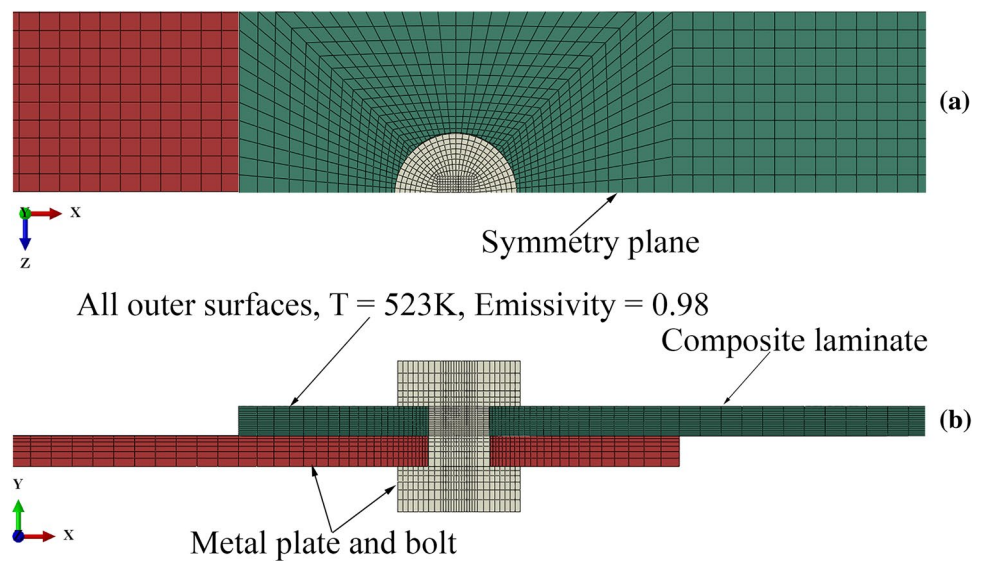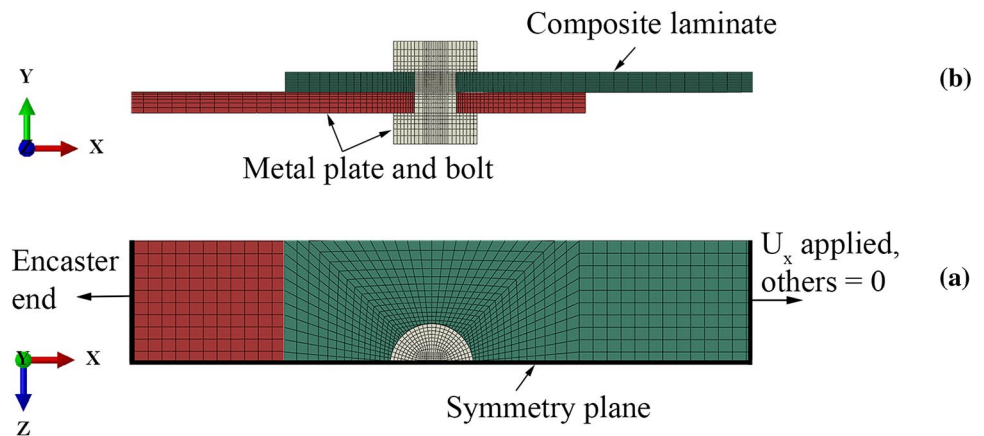

Fig. 5 Structural finite element model details **a** top view and **b** front view

C3D8R has three degrees of freedom, namely U_X, U_Y and U_Z.

There were a total of 64,128 elements in a finite element model. A region around the bolt hole and the overlap areas of metal plate/composite laminates are most important in terms of interactions of different parts and load transfer, so these regions finely meshed. To facilitate easy and detailed analysis of damage in each layer, the composite laminate is divided into 16 layers having a thickness of 0.15 mm in the thickness direction. Each layer is assigned a different material orientation with a custom material coordinate system to represent the different layup directions of each layer. For the accuracy of stress calculations, the region of contact densely meshed with one-to-one matching nodes.

Clamped boundary conditions were applied on the left end of the metal plate. Displacement loading was applied in the x direction on the right of the composite face while keeping $U_y = U_z = 0$ and $UR_x = UR_y = UR_z = 0$. Since the model was half, symmetry conditions were applied at symmetric plane XY in the global coordinate system ($U_z = 0$, $UR_x = UR_y = 0$).

4 Results

4.1 Temperature distribution in joint

Figure 6 demonstrates the temperature distribution in the joint following 1 s and 40 s. As the thermal conductivity of titanium and composite plate material is almost the same, the time required to reach uniform temperature is around 40 s as shown in Fig. 7. On the other hand, the time required for the aluminum plate to reach uniform temperature is around 2 s.
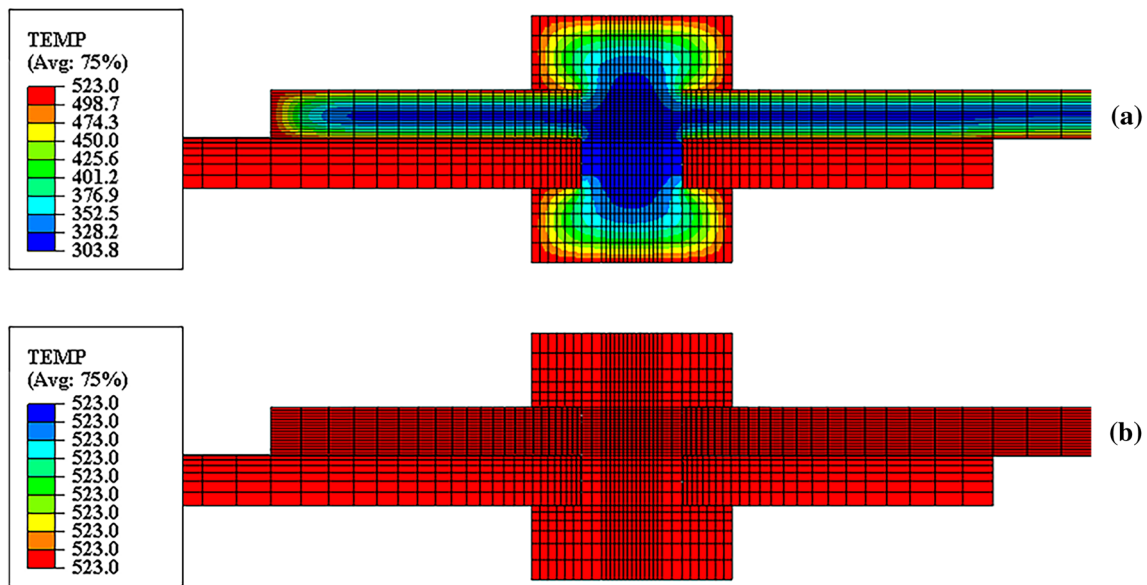
Fig. 6 Temperature distribution at different times **a** at 1 s and **b** at 40 s
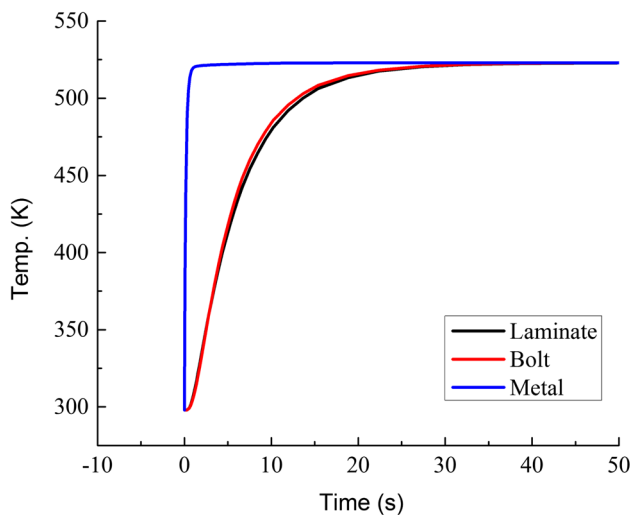

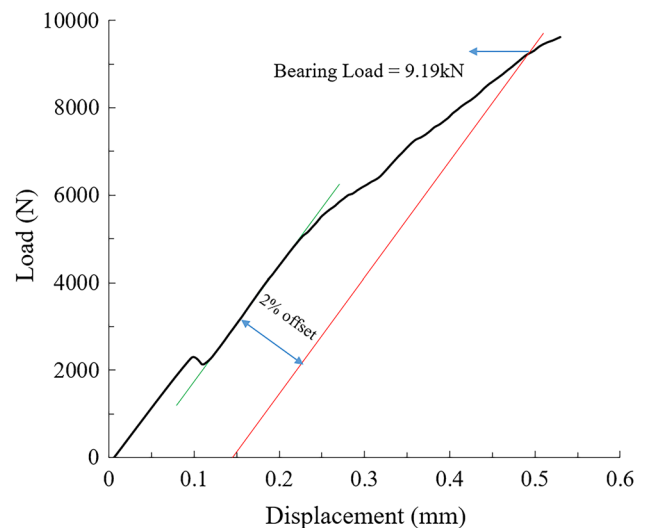**Fig. 7** Time required for aluminum plate, composite plate and bolt to reach uniform temperate

Fig. 8 Offset bearing load

4.2 Load–displacement curves

4.2.1 At room temperature

Specimens experimentally tested at room conditions are named as RT. Four specimens from group 1 and group 2 were tested at RT. The bearing load calculated by using 2% offset line according to the ASTM D5961M standard is shown in Fig. 8.

The load/displacement results are graphically plotted in Figs. 9 and 10, while Table 5 shows the 2% bearing load. The load–displacement curves show a close agreement between experimental and FEA outcomes. The percentage change between FEA and average test values for group 1 is about 2.44%, while for group 2 is about 6.62%.

4.2.2 At elevated temperature

Three specimens, from group 1 and group 2, tested at 250 °C are named as ET. Figures 11 and 12 show the load–displacement curves, while Table 6 shows the 2% bearing load. The percentage difference between FEA results and testing results is around 3.14% for group 1, while for group 2 is around 4.74%. The reduction in the offset bearing load at 250 °C for group 1 is around 42.6%, while for group 2 is around 50.4%.
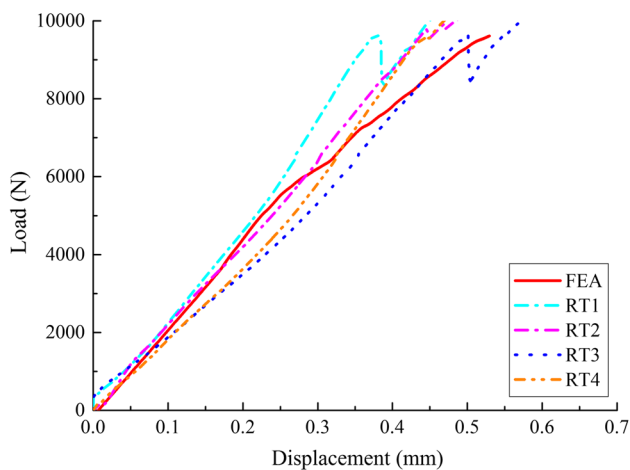
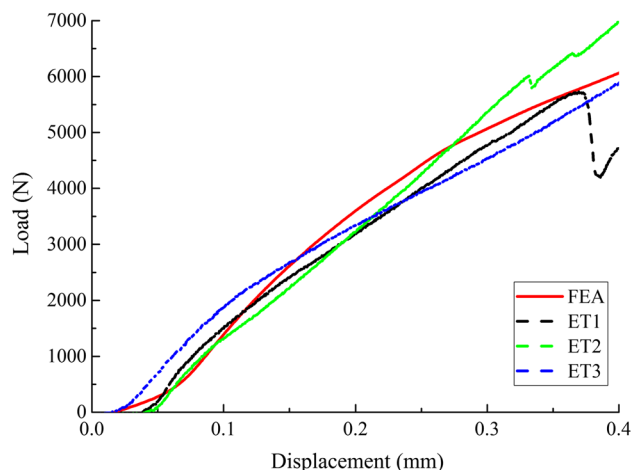**Fig. 9** Load–displacement curves at room temperature for group 1

Fig. 11 Load–displacement curves at elevated temperature for group 1
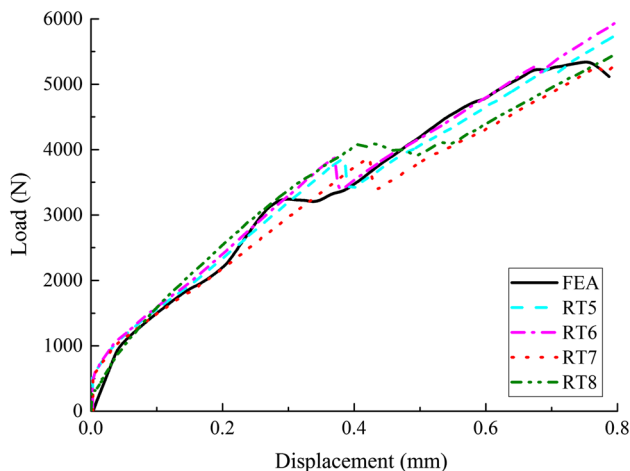

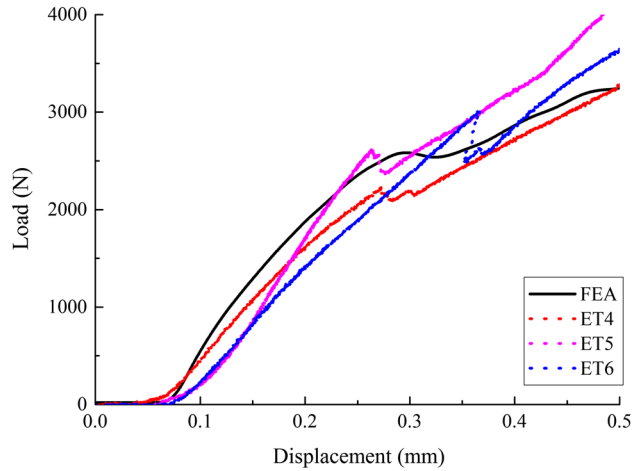**Fig. 10** Load–displacement curves at room temperature for group 2

**Fig. 12** Load–displacement curves at elevated temperature for group 2

Table 5 Offset bearing load at the room temperature

Group 1		Group 2	
Specimen	Offset bearing load (kN)	Specimen	Offset bearing load (kN)
RT1	9.46	RT5	4.71
RT2	9.87	RT6	5.57
RT3	9.23	RT7	4.31
RT4	9.10	RT8	4.15
Average	9.42	Average	4.68
FEA	9.19	FEA	4.37
Error/%	2.44	Error/%	6.62

Table 6 Offset bearing load at 250 °C

Group 1		Group 2	
Specimen	Offset bearing load (kN)	Specimen	Offset bearing load (kN)
ET1	5.06	ET4	2.27
ET2	4.97	ET5	2.32
ET3	6.20	ET6	2.38
Average	5.41	Average	2.32
FEA	5.24	FEA	2.43
Error/%	3.14	Error/%	4.74

Fig. 13 Damage in the joint **a** metal plate damage and **b** composite laminate damage

(a)　　　　　　　　　　　(b)
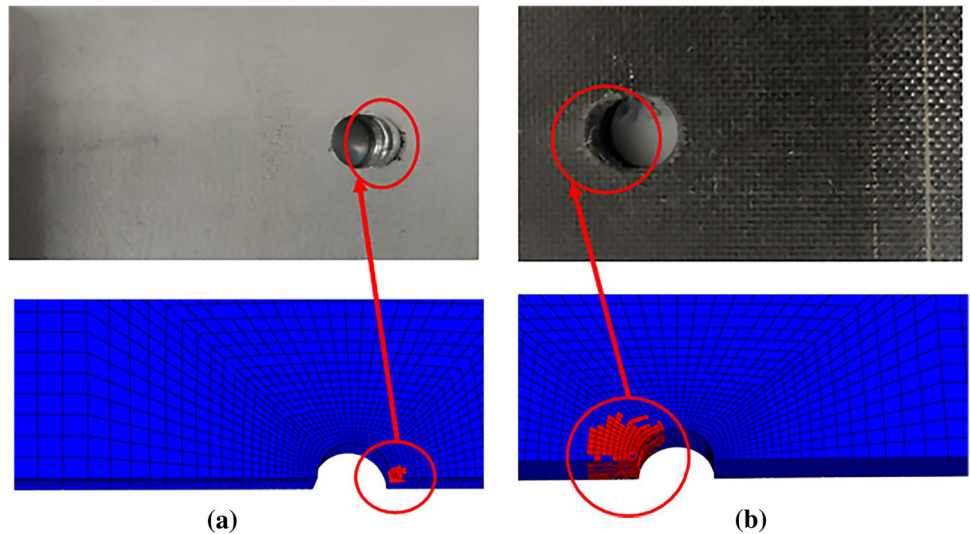
4.3 Joint failure

The joint failed due to contact pressure between the bolt and the composite laminate hole. Figure 13 shows the damage made to the laminate and metal plate. The composite laminate was damaged near the bolt hole owing to fiber/matrix shear failures. The yielding of the metal plate was also observed around the hole on the compressive side of the plate. The damage in composite laminate was made throughout the cross section near the hole at the compression side of the laminate. There was no evident yielding damage in the bolt.

4.4 Damage progression

Fiber–matrix shear damage occurred at 45° and 0° plies. The damage started near the compressive side of the hole and propagated toward the circumferential and longitudinal side. As the damage stretched in the transverse direction, it propagated toward the longitudinal side of the laminate. Fiber tensile and compressive damage occurred in 0° and −45° plies in the same location as the damage due to fiber/matrix shear and it followed the same propagation behavior.

Matrix damages started at 90° and 45° plies near the hole at uncompressed regions experiencing tensile stress. As the adhesive damage occurred, it propagated toward the compression side plies and spread to all plies.

Delamination started near the hole, and once the adhesive near the hole is completely damaged, it propagated to other plies with the propagation of extrusion of the bolt hole. The delamination damage occurred in both tension and compression regions. Figure 14 shows the damage profiles at the start of damage, while Fig. 15 shows the damage profiles at 2% bearing strength.
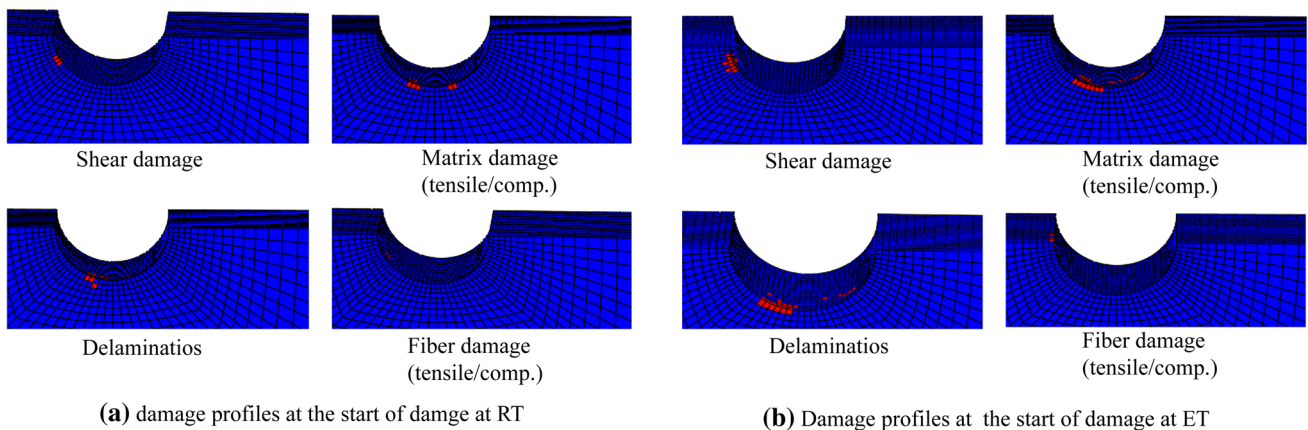

Shear damage　Matrix damage (tensile/comp.)

Delaminatios　Fiber damage (tensile/comp.)

(a) damage profiles at the start of damge at RT

Shear damage　Matrix damage (tensile/comp.)

Delaminatios　Fiber damage (tensile/comp.)

(b) Damage profiles at the start of damage at ET

Fig. 14 Damage profile at the start of damage **a** at RT and **b** at ET

(a) damage profiles at off-set bearing strength at RT

(b) Damage profiles at the off-set bearing strength at ET
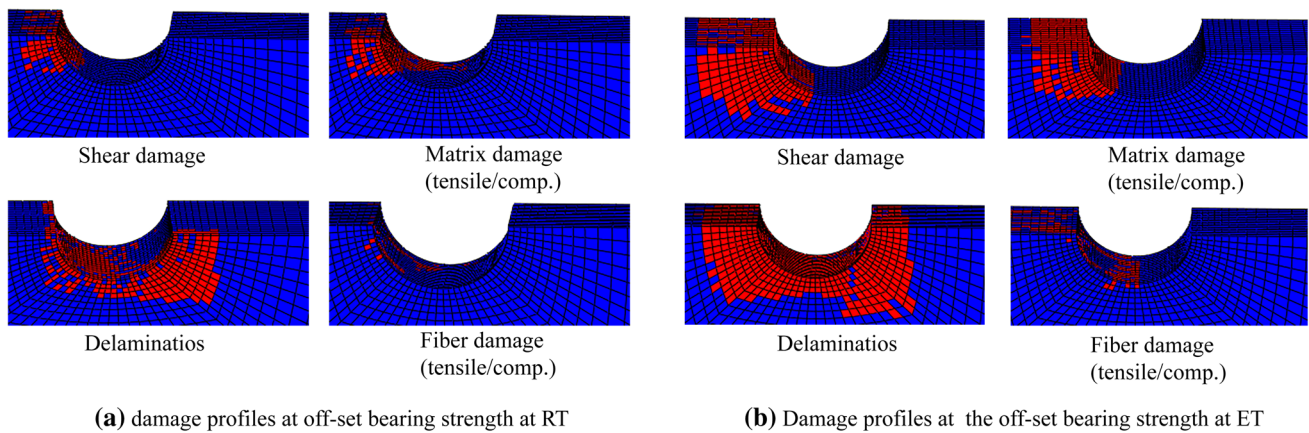
Fig. 15 Damage profiles at the offset bearing strength **a** at RT and **b** at ET

Table 7 Material properties of bolts

Material property	Titanium Value	Aluminum Value
Young modulus (GPa)	110	70.6
Density (kg/m^3)	4430	2810
Yield strength (MPa)	825	356
Thermal expansion coefficient ($\times 10^{-6}$/°C)	8.6	21.6
Thermal conductivity (W/m °C)	6.7	130

5 Discussion

5.1 The effect of bolt material

Bolt material effects on bearing strength were studied with two different materials, namely titanium and aluminum. The material properties of bolts used for strength evaluation are given in Table 7, while Fig. 16 shows the results. From results, it is clear that for both room temperature and 250 °C, bearing strength of composite connection with the aluminum bolt is less than that of titanium bolted joint. One of the reasons for this difference in bearing strength is that the better stiffness, strength and expansion coefficient of the titanium material bolt make it withstand with the higher load without damage. Replacement of titanium bolt with aluminum decreases the bearing strength around 13% at 250 °C and around 15% at room temperature. At room temperature, the stiffness of the composite and metal plate is very high that favors the higher change in bearing strength.
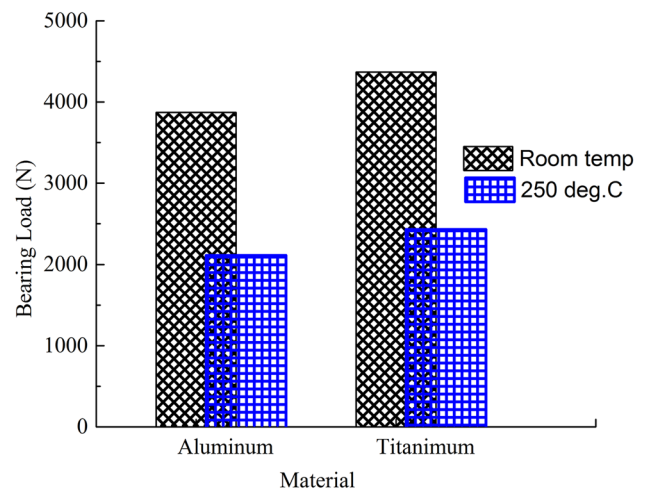

Fig. 16 Effect of bolt material on bearing strength

5.2 The effect of the thickness of composite plate

Three values of laminate thickness (such as 2.4, 3 and 4.5 mm) were used to investigate the combined effect of the thickness of composite laminate and temperature on bearing strength. Figure 17 shows the effect of the laminate thickness on crushing strength. From the results, with the increase in the thickness of the composite plate, bearing strength of joint increases proportionally. This increase in strength is more obvious for 3 mm thickness of the composite laminate than for 4.5 mm. The reason for this is that after a certain increase in the thickness of the composite plate, bearing strength greatly starts depending on the strength of the bolt and the metal plate.
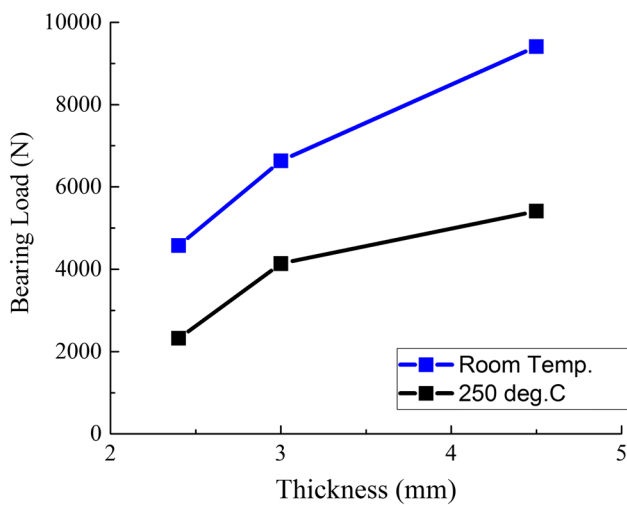
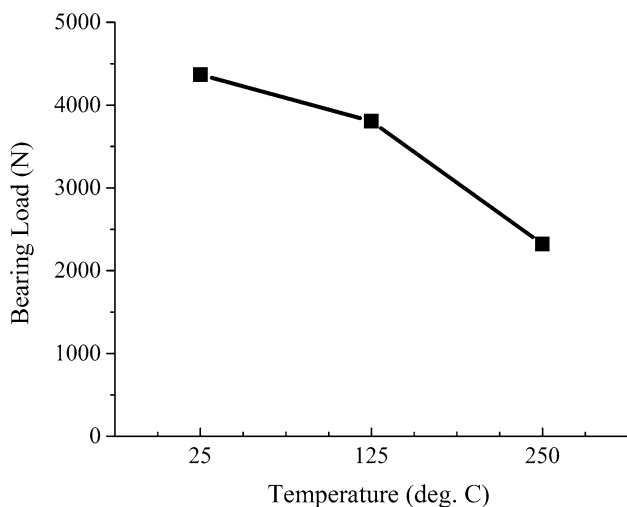**Fig. 17** Effect of thickness of laminate on bearing strength

Table 8 Stacking sequences used for analysis

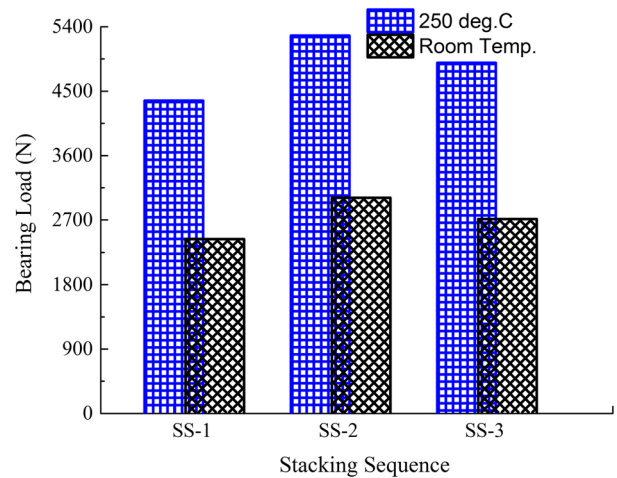| Specimen #	Stacking sequence	Bearing strength (MPa)	Ply composition (%)		
			0°	±45°	90°
SS-1	$[0_2/\pm45/0_2/90/0]_S$	202.6	62.5	25	12.5
SS-2	$[\pm45/0_2/\pm45/90/0]_s$	250.8	37.5	50	12.5
SS-3	$[0_2/\pm45_2/90_2]_S$	225.9	25	50	25

Fig. 19 Effect of stacking arrangement on bearing strength

Fig. 19 shows the effect of stacking arrangements and temperature on joint bearing strength. For this joint, bearing strength rises with the increase of 0° as well as with ±45° plies. Increasing 0° plies and decreasing ±45° plies will have a negative effect on bearing strength as is evident from SS-1. Similarly, increasing ±45° plies and decreasing 0° plies will have a negative effect as evident from SS-3. The variation in offset bearing strength at 250 °C is from 11 to 24%, while at room temperature, is from 8 to 20%. Among the three ply sequences chosen, the SS-2 is the optimal choice.

6 Conclusions

In this article, the offset bearing strength of metal-to-composite bolted joints was studied at RT and ET. The numerical models were developed in Abaqus/Standard and achieved a good promise with experimental results. The combined effects of temperature, bolt material, the thickness of the composite plate and stacking sequence were investigated. From the results, the following conclusions were obtained.

1. At high temperature, because of mismatch of thermal expansion coefficient between different parts used in

Fig. 18 Effect of temperature on bearing strength

5.3 The effect of temperature

Three different temperatures were chosen for the study of temperature effects on joint bearing strength. Figure 18 shows, as the environment temperatures increase, the bearing strength of joint decreases. There is around 13% decrease in bearing strength at 125 °C while about 50% decrease in bearing strength at 250 °C.

5.4 The effect of stacking sequence

Three different ply stacking sequences were used to study the effect of stacking sequence and temperature. Stacking arrangements investigated are tabulated in Table 8, while

composite bolted joints and change in material properties, the temperature has a major effect on the tensile properties of the joint. There is about a 50% decrease in bearing strength at 250 °C as compared to room temperature.

2. The bolt material significantly affects bearing strength of the joints. Replacement of the titanium bolt with the aluminum decreases the bearing strength around 15% at room temperature and around 13% at 250 °C.

3. Stacking sequence in combination with high temperature has a little more effect on bearing strength than stacking sequence at room temperature. The variation of offset bearing strength at 250 °C is from 11 to 24%, while at room temperature, the variation is from 8 to 20%. An increase in both $\pm 45°$ and $0°$ plies increases the bearing strength of the joint. The most suitable stacking sequence among the investigated stacking sequences is $[\pm 45/0_2/\pm 45/90/0]_s$.

References

1. Baker A, Dutton S, Kelly D (2004) Composite materials for aircraft structures, 2nd edn. AIAA Inc., Reston
2. Wang S, Zhang J, Cheng X, Cheng Y, Zhang J, Huang W (2016) Effect of damage on failure mode of multi-bolt composite joints using failure envelope method. Compos Struct 160:8–15
3. Wang S, Liu S, Liu P, Cheng X, Cheng Y (2015) Numerical analysis of bearing failure in countersunk composite joints using 3D explicit simulation method. Compos Struct 138:30–39
4. Cooper C, Turvey GJ (1995) Effects of joint geometry and bolt torque on the structural performance of single bolt tension joints in pultruded GRP sheet material. Compos Struct 32(1–4):217–226
5. Chutima S, Blackie AP (1996) Effect of pitch distance, row spacing, end distance and bolt diameter on multi-fastened composite joints. Compos A Appl Sci Manuf 27(2):105–110
6. Park HJ (2001) Effects of stacking sequence and clamping force on the bearing strengths of mechanically fastened joints in composite laminates. Compos Struct 53(2):213–221
7. Baig Y, Cheng X, Hasham HJ, Abbas M, Khan WA (2016) Failure mechanisms of scarf-repaired composite laminates under tensile load. J Braz Soc Mech Sci Eng 38(7):2069–2075
8. Gill R, Kumar V, Choudhary A (2014) Failure analysis of bolted composite joint—a review. Int J Eng Trends Technol 11(10):482–488
9. Ascione F, Feo L, MacEri F (2010) On the pin-bearing failure load of GFRP bolted laminates: an experimental analysis on the influence of bolt diameter. Compos B Eng 41(6):482–490
10. Wang SW, Cheng XQ, Guo X, Li X, Chen G (2016) Influence of lateral displacement of the grip on single lap composite-to-aluminum bolted joints. Exp Mech 56(3):407–417
11. Sen F, Sayman O (2009) Experimental failure analysis of two-serial-bolted composite plates. J Appl Polym Sci 113(1):502–515
12. Zhou S, Wang Z, Zhou J, Wu X (2013) Experimental and numerical investigation on bolted composite joint made by vacuum assisted resin injection. Compos B Eng 45(1):1620–1628
13. McCarthy MA, McCarthy CT, Padhi GS (2006) A simple method for determining the effects of bolt-hole clearance on load distribution in single-column multi-bolt composite joints. Compos Struct 73(1):78–87
14. Inal O, Balıkoglu F, Ataş A (2018) Bolted joints in quasi-unidirectional glass-fibre NCF composite laminates. Compos Struct 183:536–544
15. Kumar TVV, Shankar GSS, Shankar BL (2017) Experimental study on effect of stacking sequence, clearance and clamping torque on strength of FRP composite bolted joints. Mater Today Proc 4(10):10746–10750
16. Zu S, Zhou Z, Zhao Y, Zhang J, Zhang J (2017) Effect of temperature and geometrical parameters on mechanical properties of pin-loaded fiber metal laminate joints. J Compos Mater 51(22):3163–3173
17. Zhang J, Xu J, Lu X, Hu N, Liu F, Zhao L (2017) An interpretation of the load distributions in highly torqued single-lap composite bolted joints with bolt-hole clearances. Compos B Eng 138:194–205
18. Chani KS, Saini JS, Bhunia H (2018) Effect of nanoclay and bolt preloads on the strength of bolted joints in glass epoxy nanocomposites. J Braz Soc Mech Sci Eng 40(4):184
19. Soykok IF, Sayman O, Ozen M, Korkmaz B (2013) Failure analysis of mechanically fastened glass fiber/epoxy composite joints under thermal effects. Compos B Eng 45(1):192–199
20. Turvey GJ, Sana A (2016) Pultruded GFRP double-lap single-bolt tension joints—temperature effects on mean and characteristic failure stresses and knock-down factors. Compos Struct 153:624–631
21. Kradinov V, Madenci E, Ambur DR (2007) Combined in-plane and through-the-thickness analysis for failure prediction of bolted composite joints. Compos Struct 77(2):127–147
22. Wang HS, Hung CL, Chang FK (1996) Bearing failure of bolted composite joints. Part I: experimental characterization. J Compos Mater 30(12):1284–1313
23. Zhang J, Ma Z, Cheng X, Chen G (2012) Finite element model and load distribution analysis for three-bolted single-lap composite joints. Fuhe Cailiao Xuebao/Acta Mater Compos Sin 29(3):179–183
24. Tan SC, Perez J (1993) Progressive failure of laminates composites with a hole under compressive loading. Eng Fract Mech 45(4):529–546
25. Chang KY, Llu S, Chang FK, Liu S, Chang FK (1991) Damage tolerance of laminated composites containing an open hole and subjected to tensile loading. J Compos Mater 25(3):274–301
26. Tsai SW, Wu EM (1972) A general theory of strength for anisotropic materials. Tech Report AFML
27. Hashin Z (1980) Failure criteria for unidirectional fiber composites. J Appl Mech 47(2):329–334
28. Camanho PP, Matthews FL (1999) A progressive damage model for mechanically fastened joints in composite laminates. J Compos Mater 33(24):2248–2280
29. Tserpes KI, Labeas G, Papanikos P, Kermanidis T (2002) Strength prediction of bolted joints in graphite/epoxy composite laminates. Compos B Eng 33(7):521–529
30. Tan SC (1991) A progressive failure model for composite laminates containing openings. J Compos Mater 25(5):556–577